Electromagnetic-Thermal Analysis of Axial-Flux Permanent Magnet Eddy Current Couplers with Sub-loop Calculation Method

Dazhi Wang[1], Di Zheng[1]*, Shuo Li[1], Zhao Li[1], Bingxue Liang[1], and Yongliang Ni[2]

[1]School of Information Science and Engineering, Northeastern University, Shenyang 110819, China
[2]China North Vehicle Research Institute, Beijing 100072, China

In this paper, a precise electromagnetic–thermal model of axial-flux permanent magnet (PM) eddy current couplers is proposed to calculate the eddy current loss and predict the copper plate node temperature. With sub-loop calculation method, the quasi 3-D electromagnetic field analytical model is established in cylindrical coordinate. Based on the electromagnetic field analytical model, magnetic field distribution, eddy current losses of PM, copper plate and copper back iron are analyzed under various loads. The eddy current loss of each loop in the copper plate is calculated, at the rated slip speed. Then, the thermal resistance network is carried out, in which the previously obtained eddy current losses are heat sources for calculating the copper plate node temperature. In the thermal study, the influence of various loads on copper plate node temperature rise is analyzed. Finally, the analytical predicted results are compared with the results of finite element method and measurement. The comparison results confirm the validity of the electromagnetic–thermal model.

Keywords : axial-flux permanent magnet eddy current couplers, eddy current loss, electromagnetic–thermal model

1. Introduction

Axial-flux permanent magnet (PM) eddy current couplers are developed to transmit torque between the primary side and the output side without any mechanical friction. They have significant advantages such as soft starting of the load, vibration isolation, natural protection against overload, tolerance to shaft misalignment and so on [1-3]. The working principle of axial-flux PM eddy current couplers is based on the interaction between magnetic field induced by eddy currents in a moving conductor plate with PM magnetic field. The eddy currents are used to generate torque directly, and the induced eddy currents lead to loss and temperature rise in turn. For ensuring the safety operation, it's very necessary to perform the electromagnetic-thermal analysis, which takes the change of material characteristics under temperature.

For axial-flux PM eddy current couplers, most of the published studies are focused on the torque analysis [3-8], ignoring the eddy current loss prediction. Although the PM loss and the copper back iron loss are usually smaller

than the eddy current loss in the copper plate, they may cause significant temperature rise, which in turn may cause irreversible demagnetization of PMs. Consequently, it is essential to consider the eddy current losses of PM, copper plate and copper back iron. The magnetic field distribution is the foundation for the eddy current loss prediction. The methods are mainly analytical method based on magnetic field calculation and finite element method (FEM). Although FEM is effective for precise calculation, it is quite time consuming for mass design. Therefore, the analytical method based on the Poisson's and Laplace's equations, is explicit dependence on design parameters, provides a physical insight, and can be used as a fast analysis tool in preliminary design stages.

In fact, there is a strong interaction between electromagnetic and thermal analysis. All kinds of losses generated in electromagnetic field are the sources of heat. The temperature rise affects the electromagnetic field distribution and loss in turn. Overheat is one of the biggest problems for the axial-flux PM eddy current couplers, which can cause irreversible demagnetization of PMs. Therefore, in order to ensure a successful design and a long working life, it is necessary to focus on the electromagnetic-thermal analysis to predict loss and temperature distribution accurately. Such studies coupling the electro-

*Corresponding author: Tel: +86-188-4249-5416
Fax: +86-188-4249-5416, e-mail: zhengdivip@126.com

magnetic field and the temperature field are often analyz-ed in PM motors [9-11]. However, for PM eddy current couplers, the thermal analysis usually receives less attention than the magnetic analysis. Di Zheng et al. have done a 3-D magnetic field analytical model for the eddy current loss calculation, and the copper plate temperature prediction [12]. However, the analytical model in [12] only consider the eddy current loss of copper plate, the change of PM and iron material characteristics with the raise in temper-ature is ignored. As a result, the inaccurate results cannot meet the desirable requirements. To obtain accurate results, PM loss, copper back iron loss and the changes about material properties should be taken into consideration. The thermal analysis methods are FEM and analytical method. Compared with FEM, the analytical analysis based on thermal network model, has clear physical meaning, less computation time.

In this paper, a precise electromagnetic–thermal model of axial-flux PM eddy current couplers, which takes the change of PM, iron and copper material characteristics under temperature, is presented to calculate the eddy current loss and predict the copper plate node temperature. In Section 2, firstly the eddy current losses of PM, copper and copper back iron (P_{PM}, P_{copper}, $P_{backiron}$) are calculated by the quasi 3-D analytical model, which is based on the magnetic field calculation using sub-loop calculation method. Secondly, the thermal resistance network is developed in steady state conditions, considering heat conduction and heat convection. Thirdly, the electro-magnetic-thermal coupled analysis is done, which takes the change of material characteristics under temperature. In Section 3, firstly the magnetic field distribution in the middle of the air gap is analyzed. Secondly, the eddy current loss (P_{PM}, P_{copper}, $P_{backiron}$) with various loads are analyzed. And the eddy current loss of the each loop copper is calculated along radius direction. Thirdly, the change of copper temperature with radius is analyzed and compared with reference [12]. Under variable loads, the calculated results of the analytical thermal network model temperature are compared with FEM and measurement. In Section 4, the conclusion is presented.

2. Electromagnetic-Thermal Field Calculation

2.1. Electromagnetic Field Analysis

The axial-flux PM eddy current coupler is composed of a double rotor structure, copper side and PM side, shown in Fig. 1. Copper side includes copper and associated back iron, which is attached to the prime mover. It has the same angular velocity with prime mover. PM side is
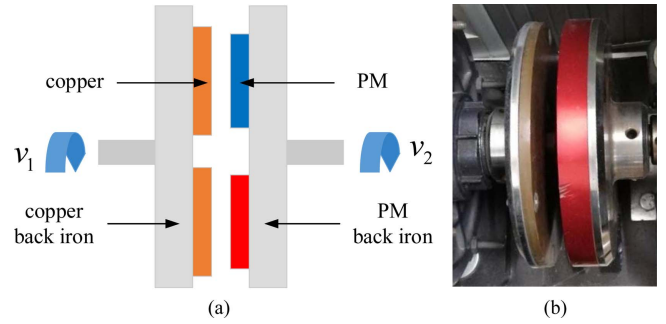

Fig. 1. (Color online) (a) Structure of the axial-flux PM eddy current coupler, (b) prototype of the axial-flux PM eddy cur-rent coupler.

consisted of PM and corresponding back iron attached to the load, has a slip speed to copper side. The eddy currents, induced in the copper side, interact with the magnetic field and generate torque.

The analytical model is established in cylindrical coordi-nate, and the sketch is shown in Fig. 2. There are five layers: PM back iron (region 1), PM (region 2), air gap (region 3), copper (region 4) and copper back iron (region 5), respectively. The conductivity of PM back iron is assumed to be zero. Due to no relative speed to the PM, there is no eddy current induced in the PM back iron [13].

To simplify the analytical model, some reasonable assumptions are adopted as follows.

(1) The axial-flux PM eddy current couplers operate in the steady state with constant slip speed, v is the slip speed between the two disks ($v = v_1-v_2$), and the slip speed is limited between 58.2 rpm and 100 rpm, which 58.2 rpm is the rated slip speed. The rated condition is that slip equals to 0.04. The speed of the primary side is 1455 rpm, so the rated slip speed is 58.2 rpm;

(2) The values of relative permeability of PM and copper are equal to 1.

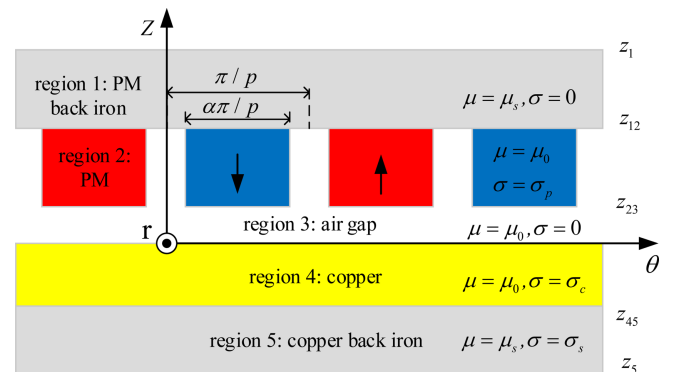(3) The back iron is composed of linear media.

Fig. 2. (Color online) Analytical model of the axial-flux PM eddy current coupler.

The magnetic vector potential **A** is defined as $\mathbf{B} = \nabla \times \mathbf{A}$, as $\nabla \cdot \mathbf{A} = 0$, there is

$$\nabla \times \mathbf{B} = -\nabla^2 \mathbf{A} \tag{1}$$

In the PM region, there is a relationship written as

$$\mathbf{B} = \mu_0 (\mathbf{H} + \mathbf{M}) \tag{2}$$

where **B** is the magnetic induction vector, **H** is the magnetic field intensity vector, **M** is the remanent magnetization vector.

As $\nabla \times \mathbf{H} = \mathbf{J}$, taking (2) into (1), there is

$$\nabla^2 \mathbf{A} = -\mu_0 (\mathbf{J} + \nabla \times \mathbf{M}) \tag{3}$$

The remanent magnetization $\mathbf{M_{zn}}$ is described as

$$\mathbf{M_{zn}}(\theta) = \sum_{n=1,3,5\ldots} \mathbf{M_{zn}}(\theta) = \sum_{n=1,3,5\ldots} M'_{zn}(\theta) e^{-i\beta\theta} \mathbf{e_z} \tag{4}$$

$$M'_{zn}(\theta) = \frac{4B_r}{\mu_0 n\pi} \sin\left(\frac{n\pi}{2}\alpha\right) \tag{5}$$

where $M_{zn}(\theta)$ is the Fourier coefficient of the nth-order axial magnetization component, $\beta = np$, p is the number of PM pairs, B_r is the remanent induction of PM.

In order to improve the accuracy of the model, the sub-loop calculation method is used, which is the copper plate is divided into N rings along radial direction, and then each ring is analyzed. The eddy current of the copper is calculated with sub-loop method, shown in Fig. 3.

Laplace's equations and Poisson's equations of the five regions are written as

$$\frac{1}{r^2}\frac{\partial^2 A_{r1}}{\partial \theta^2} + \frac{\partial^2 A_{r1}}{\partial z^2} = 0 \tag{6}$$

$$\frac{1}{r^2}\frac{\partial^2 A_{r2}}{\partial \theta^2} + \frac{\partial^2 A_{r2}}{\partial z^2} = \frac{\mu_0 \beta i}{r} M'_{zn}(\theta) e^{-i\beta\theta} - \mu_0 J_1 \tag{7}$$

$$\frac{1}{r^2}\frac{\partial^2 A_{r3}}{\partial \theta^2} + \frac{\partial^2 A_{r3}}{\partial z^2} = 0 \tag{8}$$
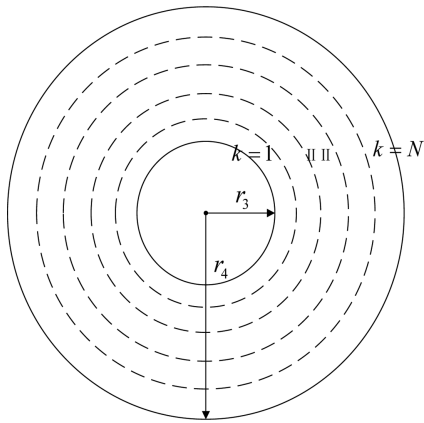

Fig. 3. Sketch of the copper plate sub-loop calculation.

$$\frac{1}{r^2}\frac{\partial^2 A_{r4}}{\partial \theta^2} + \frac{\partial^2 A_{r4}}{\partial z^2} = -\mu_0 J_k \tag{9}$$

$$\frac{1}{r^2}\frac{\partial^2 A_{r5}}{\partial \theta^2} + \frac{\partial^2 A_{r5}}{\partial z^2} = -\mu_0 \mu_s J_3 \tag{10}$$

where μ_0 is the vacuum permeability, μ_s is relative permeability of the copper back iron, J_1 and J_3 are the eddy currents induced in the PMs and the copper back iron, which are given by $J_1 = \sigma_p v B_{z2}$, $J_3 = \sigma_s v B_{z5}$, σ_p is the conductivity of PM, σ_s is the conductivity of the copper back iron, v is the slip speed. J_k is the eddy current induced in the each loop copper, $J_k = \sigma_c v B_{z4}$, σ_c is the conductivity of the copper, $k = 1,\ldots,N$, r_4 and r_4 are the inner radius and outer radius of the copper plate. In order to simplify the calculation, in the sub-loop method $N=10$.

Applying the variable separation method, the general solution to the equations of vector potentials can be expressed as

$$A_{r1} = (C_1 e^{\frac{\beta z}{r}} + D_1 e^{-\frac{\beta z}{r}}) e^{-i\beta\theta} \tag{11}$$

$$A_{r2} = (C_2 e^{\frac{\beta_1 z}{r}} + D_2 e^{-\frac{\beta_1 z}{r}}) e^{-i\beta\theta} + \left(\frac{\mu_0^2 \sigma_p v r^2}{\beta_1^2} - \frac{ir\mu_0}{\beta}\right) M'_{zn}(\theta) e^{-i\beta\theta} \tag{12}$$

$$A_{r3} = (C_3 e^{\frac{\beta z}{r}} + D_3 e^{-\frac{\beta z}{r}}) e^{-i\beta\theta} \tag{13}$$

$$A_{r4} = (C_4 e^{\frac{\beta_2 z}{r}} + D_4 e^{-\frac{\beta_2 z}{r}}) e^{-i\beta\theta} \tag{14}$$

$$A_{r5} = (C_5 e^{\frac{\beta_3 z}{r}} + D_5 e^{-\frac{\beta_3 z}{r}}) e^{-i\beta\theta} \tag{15}$$

where $\beta_1 = \sqrt{\beta^2 - i\beta\mu_0\sigma_p v r}$, $\beta_2 = \sqrt{\beta^2 - i\beta\mu_0\sigma_c v r}$ and $\beta_3 = \sqrt{\beta^2 - i\beta\mu_0\sigma_s v r}$.

The boundary conditions can be satisfied as follows, where z_1, z_{12}, z_{23}, z_{45} and z_5 are the coordinates in z direction of the interface.

$$-\frac{1}{r}\frac{\partial A_{r1}}{\partial \theta} = 0\Big|_{z=z_1} \tag{16}$$

$$-\frac{1}{r}\frac{\partial A_{r1}}{\partial \theta} = -\frac{1}{r}\frac{\partial A_{r2}}{\partial \theta}\Big|_{z=z_{12}} \quad \frac{1}{\mu_0\mu_s}\frac{\partial A_{r1}}{\partial z} = \frac{1}{\mu_0}\frac{\partial A_{r2}}{\partial z}\Big|_{z=z_{12}} \tag{17}$$

$$-\frac{1}{r}\frac{\partial A_{r2}}{\partial \theta} = -\frac{1}{r}\frac{\partial A_{r3}}{\partial \theta}\Big|_{z=z_{23}} \quad \frac{1}{\mu_0}\frac{\partial A_{r2}}{\partial z} = \frac{1}{\mu_0}\frac{\partial A_{r3}}{\partial z}\Big|_{z=z_{23}} \tag{18}$$

$$-\frac{1}{r}\frac{\partial A_{r3}}{\partial \theta} = -\frac{1}{r}\frac{\partial A_{r4}}{\partial \theta}\Big|_{z=0} \quad \frac{1}{\mu_0}\frac{\partial A_{r3}}{\partial z} = \frac{1}{\mu_0}\frac{\partial A_{r4}}{\partial z}\Big|_{z=0} \tag{19}$$

$$-\frac{1}{r}\frac{\partial A_{r4}}{\partial \theta} = -\frac{1}{r}\frac{\partial A_{r5}}{\partial \theta}\Big|_{z=z_{45}} \quad \frac{1}{\mu_0\mu_s}\frac{\partial A_{r4}}{\partial z} = \frac{1}{\mu_0}\frac{\partial A_{r5}}{\partial z}\Big|_{z=z_{45}} \tag{20}$$

$$-\frac{1}{r}\frac{\partial A_{r5}}{\partial \theta} = 0\Big|_{z=z_5} \tag{21}$$

The distribution of magnetization components are taken into the boundary conditions, and the vector potentials A_{r1}, A_{r2}, A_{r3}, A_{r4} and A_{r5} are obtained as

$$A_{r1} = \sum_{n=1,3,5\ldots} \frac{e^{\frac{\beta z_{12}}{r}}(e^{\frac{\beta z_{12}}{r}} - e^{-\frac{\beta z_{12}}{r}})E_1 M}{e^{\frac{\beta z_{23}}{r}}(e^{\frac{2\beta z_1}{r}} - e^{\frac{2\beta z_{12}}{r}})E_2}(e^{\frac{\beta z}{r}} + e^{\frac{2\beta z_1 + \beta z}{r}})e^{-i\beta\theta} \quad (22)$$

$$A_{r2} = \sum_{n=1,3,5\ldots}(E_8 e^{\frac{\beta_1 z}{r}} + E_9 e^{-\frac{\beta_1 z}{r}} + 1)M e^{-i\beta\theta} \quad (23)$$

$$A_{r3} = \sum_{n=1,3,5\ldots} \frac{-\beta(e^{\frac{2\beta z_{12}}{r}} - e^{\frac{2\beta z_{23}}{r}})M}{e^{\frac{\beta z_{23}}{r}}E_2}(E_3 e^{\frac{\beta z}{r}} + E_4 e^{\frac{\beta z}{r}})e^{-i\beta\theta} \quad (24)$$

$$A_{r4} = \sum_{n=1,3,5\ldots} \frac{-\beta(e^{\frac{2\beta z_{12}}{r}} - e^{\frac{2\beta z_{23}}{r}})M}{e^{\frac{\beta z_{23}}{r}}E_2}(e^{\frac{\beta z}{r}} + e^{\frac{2\beta_2 z_{45} + \beta z}{r}})e^{-i\beta\theta} \quad (25)$$

$$A_{r5} = \sum_{n=1,3,5\ldots} \frac{-2e^{\frac{\beta_2 z_{45} + \beta_3 z_{45}}{r}}\beta(e^{\frac{2\beta z_{12}}{r}} - e^{\frac{2\beta z_{23}}{r}})}{e^{\frac{2\beta z_{23}}{r}}E_2}M(e^{\frac{\beta z}{r}} - e^{\frac{2\beta_3 z_5 + \beta z}{r}})e^{-i\beta\theta} \quad (26)$$

where E_1, E_2, E_3, E_4, E_5, E_6, E_7, E_8, E_9, M are given in the appendix.

The circumferential and axial components of the flux density distribution in the air gap are

$$B_{\theta 3} = \frac{\partial A_{r3}}{\partial z} = \sum_{n=1,3,5\ldots} \frac{-\beta^2(e^{\frac{2\beta z_{12}}{r}} - e^{\frac{2\beta z_{23}}{r}})M}{re^{\frac{\beta z_{23}}{r}}E_2}(E_3 e^{\frac{\beta z}{r}} + E_4 e^{\frac{\beta z}{r}})e^{-i\beta\theta} \quad (27)$$

$$B_{z3} = -\frac{1}{r}\frac{\partial A_{r3}}{\partial \theta} = \sum_{n=1,3,5\ldots} \frac{-i\beta^2(e^{\frac{2\beta z_{12}}{r}} - e^{\frac{2\beta z_{23}}{r}})M}{re^{\frac{\beta z_{23}}{r}}E_2}(E_3 e^{\frac{\beta z}{r}} + E_4 e^{\frac{\beta z}{r}})e^{-i\beta\theta} \quad (28)$$

The eddy current density induced in PM, copper and copper back iron can be expressed as

$$J_1 = \sum_{n=1,3,5\ldots} \frac{i\beta\sigma_p v}{r}(E_8 e^{\frac{\beta_1 z}{r}} + E_9 e^{-\frac{\beta_1 z}{r}} + 1)M e^{-i\beta\theta} \quad (29)$$

$$J_k = \sum_{n=1,3,5\ldots} \frac{-i\beta^2\sigma_c v(e^{\frac{2\beta z_{12}}{r}} - e^{\frac{2\beta z_{23}}{r}})M}{e^{\frac{\beta z_{23}}{r}}E_2 r}(e^{\frac{\beta z}{r}} + e^{\frac{2\beta_2 z_{45} + \beta z}{r}})e^{-i\beta\theta} \quad (30)$$

$$J_3 = \sum_{n=1,3,5\ldots} \frac{-i\beta^2\sigma_s v2e^{\frac{z_{45}(\beta_2+\beta_3)}{r}}(e^{\frac{2\beta z_{12}}{r}} - e^{\frac{2\beta z_{23}}{r}})}{e^{\frac{2\beta z_{23}}{r}}E_2 r}M(e^{\frac{\beta z}{r}} - e^{\frac{2\beta_3 z_5 + \beta z}{r}})e^{-i\beta\theta} \quad (31)$$

Taking into account the actual eddy current paths, an effective Russell–Norsworthy (R–N) factor is introduced [14], the dissipated eddy current power P_{PM}, P_{copper} and $P_{back\,iron}$ in the PM, the copper and the copper back iron

can be obtained by (32), (33) and (34), where r_1 and r_2 are the inner radius and outer radius of the PM, L_1 is the length of PM in radius direction.

$$P_{PM} = \frac{k_s}{\sigma_p}\int_{z_{23}}^{z_{12}}\int_0^{2\pi}\int_{r_1}^{r_2}\alpha|J_1|^2 rdrd\theta dz \quad (32)$$

$$P_{copper} = \sum_{k=1,\ldots,9}\frac{k_s}{\sigma_c}\int_{z_{45}}^0\int_0^{2\pi}\int_{r_k}^{r_{k+1}}|J_k|^2 rdrd\theta dz \quad (33)$$

$$P_{backiron} = \frac{k_s}{\sigma_s}\int_{z_5}^{z_{45}}\int_0^{2\pi}\int_{r_3}^{r_4}|J_3|^2 rdrd\theta dz \quad (34)$$

$$k_s = 1 - \frac{\tanh(2pL_1/(r_4 - r_3))}{(2pL_1/(r_4 - r_3))(1 + (r_4 - r_3)/L_1)} \quad (35)$$

2.2. Thermal field analysis

The thermal resistances include conduction thermal resistances and convection thermal resistances, neglecting radiation resistances, in this paper. The equivalent thermal resistance network, based on T-equivalent lumped parameter, is shown in Fig. 4. And the temperature nodes can be derived from the heat transfer equations, which is the one of PM (T_1), PM back iron (T_2), air gap (T_3), aluminum (T_4), copper back iron (T_5), cooling fin (T_6) and ambient (T_7), copper (T_c), respectively. In Fig. 4, P_{PM} is the eddy current loss of the PM, $P_{back\,iron}$ is the eddy current loss of the copper back iron. $P_{copper(k)}$ is the eddy current loss of the copper in each loop $k = 1, 2,\ldots, N-1$, c
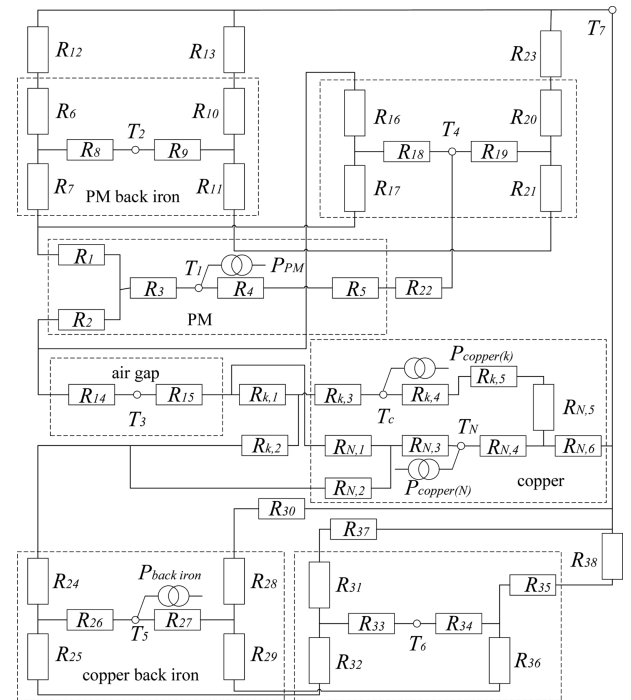

Fig. 4. Equivalent thermal resistance network of the axial-flux PM eddy current coupler.

$= k + 7$.

The general expression of conduction thermal resistances is [15]

$$R_{conduction} = \frac{L}{kA} \tag{36}$$

where L is the path length, A is the path area, k is the thermal conductivity of the material.

The conduction thermal resistances R_1-R_5, R_6-R_{11}, R_{16}-R_{21}, R_{24}-R_{29}, R_{31}-R_{36}, $R_{k,1}$-$R_{k,5}$ and $R_{N,1}$-$R_{N,5}$ can be calculated by the thermal resistance formulation of the general cylindrical component [16].

The general expression of convection thermal resistances is [10]

$$R_{convection} = \frac{1}{hA} \tag{37}$$

where h is the convection heat transfer coefficient.

For R_{12}, R_{13}, R_{23}, R_{30}, R_{37} and R_{38}, the coefficient can be estimated as a function of the air speed over the surface [17]

$$h = \frac{1 + 0.25v_k}{0.045} \tag{38}$$

where v_k is the rotational speed of the surface.

For R_{14} and R_{15}, the convection heat transfer coefficient is evaluated based on Nusselt number Nu [16]

$$h = \frac{N_u \lambda_{air}}{g} \tag{39}$$

$$N_u = 0.409 \left(\frac{v_k^2 g^3}{\gamma r_4} \right)^{0.241} \tag{40}$$

where λ_{air} is the thermal conductivity, g the length of air gap, and v_k is the relative speed of the two convection heat transfer surface, γ is the kinematic viscosity of the air.

The temperature at each node can be calculated as

$$GT = P \tag{41}$$

where T is the nodal temperature rise matrix, G is the thermal conductance matrix and P is the power loss vector.

2.3. Electromagnetic-thermal analysis

Fig. 5 gives the flow diagram of the electromagnetic-thermal model. The coupled calculation is considered via a temperature iteration process, as material characteristics vary with temperature. Firstly, the initial node temperature is set, the eddy current loss is obtained by the electromagnetic field analytical model. Secondly, the equivalent
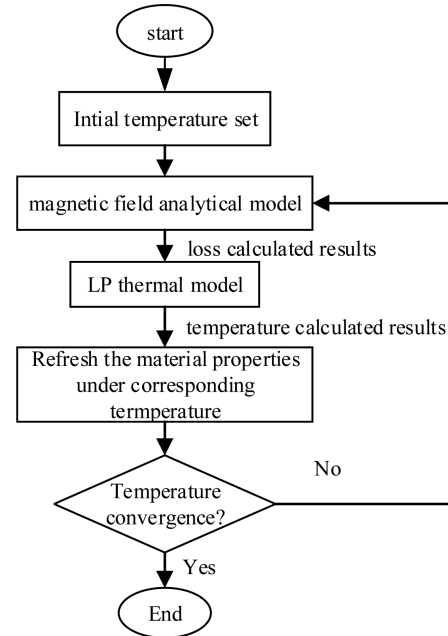

Fig. 5. Electromagnetic-thermal coupled analysis process.

thermal resistance network based on T-equivalent lumped parameter (LP), is used to calculate temperature distribution, with the heat source obtained by the electromagnetic model. Then, the new temperature of each node is determined with updated the material characteristics of PM, back iron and each loop copper under corresponding temperature. Such iterative computation loop is closed until the relative difference $\Delta T < 3\%$.

3. Result and Discussion

The main structure parameters of a 125 kW prototype with the one-side axial-flux PM eddy current coupler are

Table 1. Structure parameters.

Quantity	Value	Unit
number of the pole pairs	14	-
mean pole-arc length	38.05	mm
mean pole pitch	63.74	mm
PM thickness	31.7	mm
copper plate thickness	6.1	mm
inner radius of copper/copper back iron	209.6	mm
outer radius of copper/copper back iron	387.4	mm
radius of PM back iron	330.2	mm
copper back iron thickness	12.7	mm
PM back iron thickness	9.5	mm
air gap	3	mm
copper conductivity (20 °C)	57.1	MS/m
iron conductivity (20 °C)	6.9	MS/m
PM conductivity (20 °C)	0.625	MS/m

(a) at the mean radius

(b) at the inner radius of the copper plate

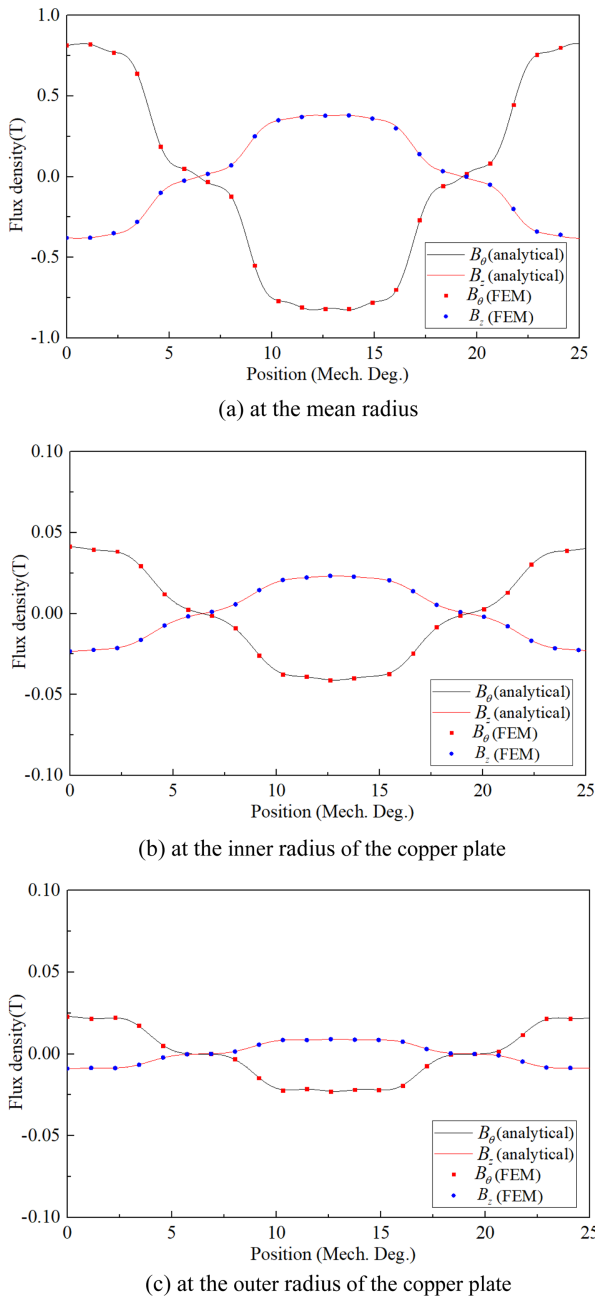(c) at the outer radius of the copper plate

Fig. 6. (Color online) Magnetic field distribution of the air gap.

shown in Table 1. The speed of the primary side is 1455 rpm, and the slip speed is a controllable variable. In order to evaluate the proposed analytical model, nonlinear 3D-FEM obtained by ANSYS Workbench 14.5 is used as the comparison.

3.1. Flux density distribution

The flux density distribution of the air gap is proposed by analytical model and FEM, under rated operating condition, which is at the slip speed of 58.2 rpm, shown

in Fig. 6. The analytical results have high accuracy according to the 3-D FEM results, and the difference is smaller than 3.85 %. It proves that the proposed analytical model is effective and can predict the magnetic field distribution accurately.

3.2. Eddy current loss

The analytical model is used to estimate the eddy current loss of the PM, the copper and the copper back iron. As the slip speed increases with the load increases, the slip speed is selected as the variable.

The axial-flux PM eddy current coupler first rotates at the rated slip speed 58.2 rpm, with the increase of the load, the eddy current loss increases rapidly. For clarity, the eddy current losses of the PM and the copper back iron are multiplied by the coefficient, in Fig. 7. In the term of the loss analysis, the eddy current loss of copper back iron can't be neglected. At large slip speed, the eddy
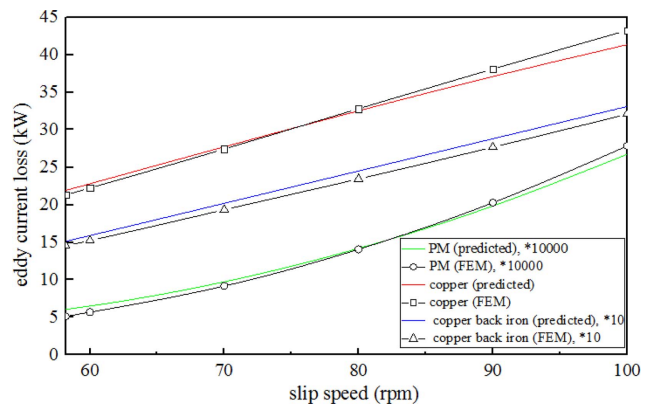

Fig. 7. (Color online) Comparison of analytical predicted and FEM results of eddy current loss of PM, copper and copper back iron.
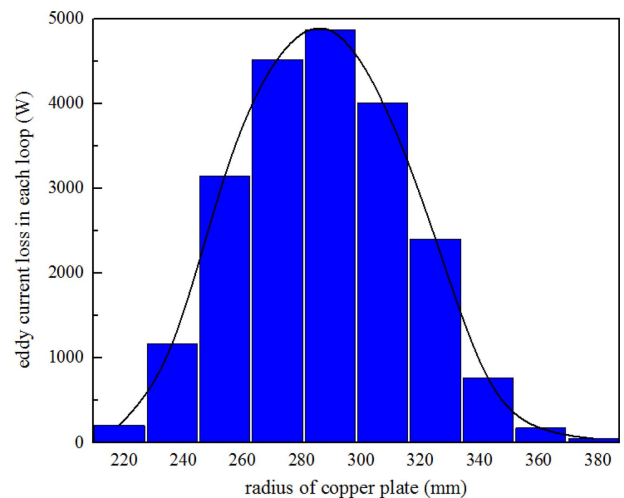

Fig. 8. (Color online) Eddy current loss of each loop with radius.

current loss of the PM can't be neglected, as the problem of PM loss and generating heat, is more obvious. In this paper, we calculate the eddy loss of PM to make sure the axial-flux PM eddy current coupler can work stably in entire working range. The eddy current loss analytical calculated results are compared with FEM results under various loads, and the difference is under 3.92 %. The analytical calculated results agree well with the FEM results, and the analytical model can reflect the influence of eddy current loss on the slip speed.

With the sub-loop calculation method, the eddy current of each copper loop can be calculated at the slip speed of 58.2 rpm, shown in Fig. 8. The copper eddy current loss distribution is inhomogeneous, the loss increases at first then decreases along the radius.

3.3. Temperature distribution

At the slip speed of 58.2 rpm, the temperature of copper plate is calculated in ANSYS Workbench 14.5, and the temperature distribution with the new cooling fin is shown in Fig. 9. At the slip speed of 58.2 rpm, using the sub-loop calculation method the temperature of the copper changes with radius is calculated and compared with [12], and the temperature change of each node is more gently, shown in Fig. 10. The analytical model in [12] only consider the eddy current loss of copper plate, the change of PM and iron material characteristics with the raise in temperature is ignored. As a result, the inaccurate results cannot meet the desirable requirements. In other words, the method in this paper is more coincident with the facts.

The testing bench for the measurements of eddy current loss and temperature is shown in Fig. 11. It is composed
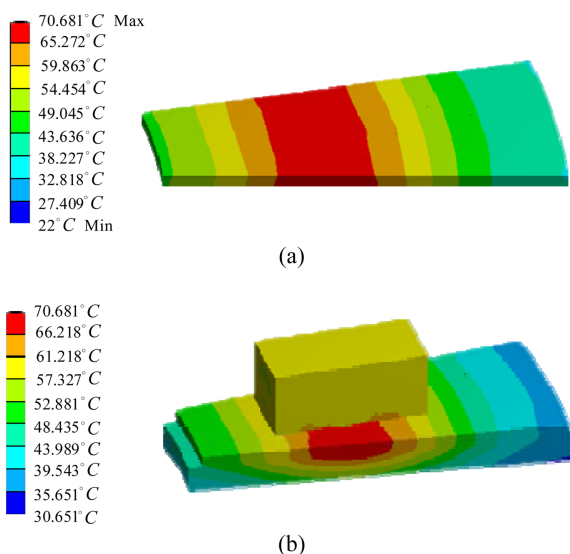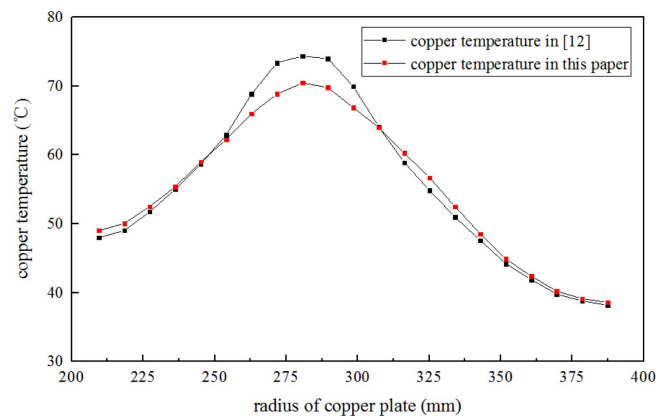

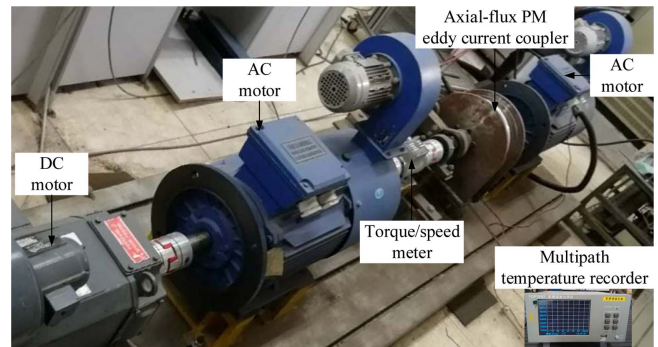**Fig. 10.** (Color online) Copper temperature changes with radius.

Fig. 11. (Color online) Test prototype diagram.

of AC motor, axial-flux PM eddy current coupler, torque/speed meter, AC motor and DC motor. The temperature is measured multipath temperature recorder. The multipath temperature recorder is used for static measurement. When temperature rising reach steady state, stop the axial-flux PM eddy current coupler, and measure temperature. The copper temperature distribution is inhomogeneous, the temperature increases at first then decreases, and it
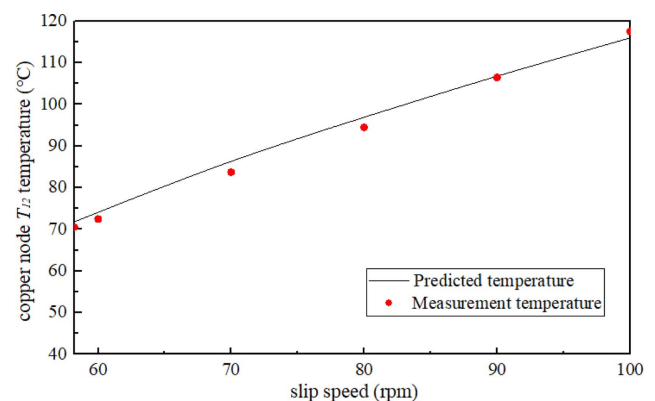

Fig. 9. (Color online) FEM calculated result of temperature distribution: (a) copper, (b) PM, copper and copper back iron.

Fig. 12. (Color online) Comparison of analytical predicted and measurement results of copper node T_{12} temperature.

reaches the top at temperature node T_{12}. Under variable loads, the calculated results of the analytical thermal network model temperature node T_{12} are compared with measurement shown in Fig. 12, and the difference is under 4.06 %. The comparison result demonstrates that the analytical result is in good agreement with the FEM and measurement results, and the analytical model can predict the node temperature accurately.

4. Conclusions

A precise electromagnetic–thermal model of axial-flux PM eddy current couplers is proposed, which takes the change of material characteristics under temperature. Under various loads, the eddy current losses of the axial-flux PM eddy current coupler are calculated, and the copper plate temperature is predicted analytically, using the electromagnetic-thermal coupled method. With the sub-loop calculation method, the eddy current of each copper loop can be calculated. In the thermal study, the influence of various loads on copper plate node temperature rise is analyzed. Furthermore, FEM and measurement are also used to verify the analytical model. The results, which are in good agreement with analytical results, indicate that the electromagnetic–thermal model is reasonable, efficient and meaningful for the design and optimization procedure.

Acknowledgments

References

[1] T. Lubin, S. Mezani, and A. Rezzoug, IEEE Trans. Energy Convers. **27**, 536 (2012).

[2] S. Mohammadi, M. Mirsalim, S. Vaez-Zadeh, and H. A. Talebi, IEEE Trans. Ind. Electron. **61**, 5940 (2014).

[3] Jian Wang, Heyun Lin, Shuhua Fang, and Yunkai Huang, IEEE Trans. Magn. **50**, 8000109 (2014).

[4] Min-Gyu Park, Jang-Young Choi, Hyeon-Jae Shin, and Seok-Myeong Jang, J. Appl. Phys. **115**, 17E707 (2014).

[5] Thierry Lubin and Abderrezak Rezzoug, IEEE Trans. Magn. **5**, 8203712 (2016).

[6] Kyoung-Chul Min, Jang-Young Choi, Jeong-Man Kim, Han-Wook Cho, and Seok-Myoeng Jang, IEEE Trans. Magn. **51**, 8110304 (2015).

[7] Thierry Lubin and Abderrezak Rezzoug, IEEE Trans. Ind. Electron. **62**, 2287 (2015).

[8] Zhao Li, Dazhi Wang, Di Zheng, and Linxin Yu, AIP Adv. **7**, 105303 (2017).

[9] Nannan Zhao and Weiguo Liu, IEEE Trans. Magn. **51**, 8112604 (2015).

[10] Hongfeng Li and Yanbo Shen, IEEE Trans. Energy Convers. **30**, 991 (2015).

[11] Yunyun Chen, Xiaoyong Zhu, and Lin Wang, IEEE Trans. Appl. Supercond. **26**, 5205305 (2016).

[12] D. Zheng, D. Wang, S. Li, T. Shi, Z. Li, and L. Yu, AIP Adv. **7**, 025117 (2017).

[13] Hyeon-Jae Shin, Jang-Young Choi, Han-Wook Cho, and Seok-Myeong Jang, IEEE Trans. Magn. **49**, 4152 (2013).

[14] R. L. Russell and K. H. Norsworthy, Proc. IEE A, Power Eng. **105**, 163 (1958).

[15] Nannan Zhao, Z. Q. Zhu, and Weiguo Liu, IEEE Trans. Magn. **47**, 4199 (2011).

[16] Naghi Rostami, Mohammad Reza Feyzi, Juha Pyrhönen, Asko Parviainen, and Markku Niemelä, IEEE Trans. Magn. **49**, 1178 (2013).

[17] Longnv, L., W. N., F. S. L., H., Shuangxia, N., and Yan, L., IEEE Trans. Ind. Electron. **62**, 6076 (2015).

Appendix

The elements of equation (22) to equation (26) are expressed as follows.

$$E_1 = (\beta(e^{\frac{2\beta_2 z_{45}}{r}} + 1)(e^{\frac{\beta(z_{12}+z_{23})}{r}} + 1) - \beta_2(e^{\frac{2\beta_2 z_{45}}{r}} - 1)(e^{\frac{\beta(z_{12}+z_{23})}{r}} - 1)) \quad (A.1)$$

$$E_2 = (\beta_2(e^{\frac{2\beta z_{12}}{r}} + 1)(e^{\frac{2\beta_2 z_{45}}{r}} - 1) - \beta(e^{\frac{2\beta z_{12}}{r}} - 1)(e^{\frac{2\beta_2 z_{45}}{r}} + 1)) \quad (A.2)$$

$$E_3 = (\beta(e^{\frac{2\beta_2 z_{45}}{r}} + 1) - \beta_2(e^{\frac{2\beta_2 z_{45}}{r}} - 1)) \quad (A.3)$$

$$E_4 = (\beta(e^{\frac{2\beta_2 z_{45}}{r}} + 1) + \beta_2(e^{\frac{2\beta_2 z_{45}}{r}} - 1)) \quad (A.4)$$

$$E_5 = (e^{\frac{2\beta_3 z_5}{r}}(e^{\frac{2\beta z_{23}+2\beta_2 z_{45}}{r}} + 1) - e^{\frac{2\beta_3 z_{45}}{r}}(e^{\frac{2\beta z_{23}+2\beta_2 z_{45}}{r}} - 1)) \quad (A.5)$$

$$E_6 = (\beta_2(e^{\frac{2\beta z_{23}}{r}} + 1)(e^{\frac{2\beta_2 z_{45}}{r}} - 1) - \beta(e^{\frac{2\beta z_{23}}{r}} - 1)(e^{\frac{2\beta_2 z_{45}}{r}} + 1)) \quad (A.6)$$

$$E_7 = (e^{\frac{2\beta z_{23}}{r}} + e^{\frac{2\beta_2 z_{45}}{r}})(e^{\frac{2\beta_3 z_{45}}{r}} + e^{\frac{2\beta_3 z_5}{r}}) \quad (A.7)$$

$$E_8 = \frac{-2e^{\frac{\beta z_{12}}{r}}(e^{\frac{2\beta z_1}{r}} + e^{\frac{2\beta z_{12}}{r}})E_3}{2u(e^{\frac{2\beta z_1}{r}} - e^{\frac{2\beta z_{12}}{r}})E_2} + \frac{((\beta+\beta_2)E_7 - (\beta-\beta_2)E_5)}{2e^{\frac{2\beta z_{23}}{r}}(e^{\frac{2\beta_3 z_{45}}{r}} - e^{\frac{2\beta_3 z_5}{r}})E_2} \quad (A.8)$$

$$E_9 = \frac{-2e^{\frac{\beta z_{12}}{r}}(e^{\frac{2\beta z_1}{r}} + e^{\frac{2\beta z_{12}}{r}})E_4}{2u(e^{\frac{2\beta z_1}{r}} - e^{\frac{2\beta z_{12}}{r}})E_2} + \frac{e^{\frac{2\beta z_{12}}{r}}E_6}{2e^{\frac{\beta z_{23}}{r}}E_2} \quad (A.9)$$

$$M = \left(\frac{\mu_0^2 \sigma_p v r^2}{\beta_1^2} - \frac{ir\mu_0}{\beta}\right)M'_{zn}(\theta) \quad (A.10)$$